



# MONITOR

## Multi-Model Investigation of Tidal Energy Converter Reliability

Fostering Renewable Energies and Energy  
Efficiency

Numerical Modelling - Work Package 5  
*Improved Blade Geometry Modelling in BEMT*

Iestyn Evans  
22-12-2020



## Revision

Revision No.	Revision Text	Initials	Date
1.	<i>First draft</i>	<i>IE</i>	<i>22-12-2020</i>
2.	<i>Review of first draft</i>	<i>MT</i>	<i>12-01-2021</i>
3.	<i>Second draft</i>	<i>IE</i>	<i>15-01-2020</i>

## Project Information

<b>Project Title</b>	<i>Multi-Model Investigation of Tidal Energy Converter Reliability</i>
<b>Project Acronym</b>	<i>MONITOR</i>
<b>Project Number</b>	<i>EAPA_333/2016</i>
<b>Programme Priority &amp; Specific Objective</b>	<i>Resource Efficiency</i>
<b>Duration</b>	
<b>Month 1</b>	<i>August 2017</i>
<b>Project Manager</b>	<i>Michael Togneri — Swansea University</i>
<b>Work Package Leader</b>	<i>Iestyn Evans — Swansea University</i>
<b>Work Package Number/Name</b>	<i>WP5 — Numerical Modelling</i>

## MONITOR Consortium

<b>Organisation Name</b>	<b>Country</b>
European Marine Energy Centre	<i>UK</i>
Magallanes Renovables S.L.	<i>Spain</i>
Offshore Renewable Energy Catapult	<i>UK</i>
Region Normandie	<i>France</i>
Sabella S.A.S.	<i>France</i>
Swansea University (Lead Partner)	<i>UK</i>
Universidade Do Algarve	<i>Portugal</i>
Universite La Harve Normandie	<i>France</i>
University College Cork	<i>Ireland</i>

### Copyright notice

©2017-2021 by the MONITOR Consortium

This document contains information that is protected by copyright. All rights reserved. No part of this work covered by copyright hereon may be reproduced or used in any form without the permission of the copyright holders.

## Abstract

TSTs have the potential to become significant contributors in the generation of low carbon energy. Cost, driven mostly by planned and unplanned maintenance, is the most significant barrier limiting widespread adoption of TSTs at commercial scale. Minimising planned maintenance and reducing the chances of any unplanned maintenance will greatly improve the appeal of TSTs as generators of low carbon energy.

Accurate numerical models can be used to predict the structural loads on TSTs and help improve the reliability (and thus reduced maintenance costs) of their design. BEMT is a common numerical model that is used for design and performance evaluation of TSTs. BEMT is often the preferred numerical model as it offers acceptable accuracy for evaluation of turbine design iterations with significant computational saving.

A robust BEMT model has been developed at Swansea University, which was the foundation of this work. Previous versions of the BEMT model only allowed for constant geometry and Reynolds modelling of the turbine rotor blade, i.e, a single lift and drag curves were assigned to all elements across the radius of the rotor blade. No real rotor blade has a constant blade profile and Reynolds Number across its radius which leads to inaccuracies in the results when using the BEMT model. Implementing the capability of assigning unique lift and drag curves to each element based on its geometry and Reynolds Number in the BEMT model has improved the blade geometry modelling, and thus the turbine performance predictions.

Three different TSTs rotor blades were analysed: Magallanes ATIR, Sabella D12, and IFREMER. Results from the improved BEMT model are compared to laboratory data for all three TSTs to quantify any improvements in its prediction of rotor performance. An average improvement of 20% in predicting laboratory maximum rotor performance results is seen from the original to improved BEMT model.

Improvements in the accuracy of the BEMT model will directly enhance the design and evaluation of TSTs. A reduction in cost of TSTs will be seen with a better design which is achievable from the more accurate BEMT model. This will increase the adoption of TSTs as generators of clean renewable energy.

## Contents

<b>1</b>	<b>Introduction</b>	<b>1</b>
<b>2</b>	<b>Blade Element Momentum Theory</b>	<b>1</b>
<b>3</b>	<b>BEMT Procedure</b>	<b>3</b>
3.1	Cases . . . . .	3
3.2	Synthetic Flow Fields . . . . .	4
3.3	Implementation . . . . .	5
3.4	Calculation of Reynolds Number . . . . .	6
3.5	Creation of Lift and Drag Data . . . . .	7
3.6	Laboratory Testing . . . . .	7
<b>4</b>	<b>Magallanes ATIR</b>	<b>9</b>
4.1	Rotor Blade Description . . . . .	9
4.2	Methodology . . . . .	10
4.3	Results . . . . .	11
<b>5</b>	<b>Sabella D12</b>	<b>17</b>
5.1	Rotor Blade Geometry . . . . .	17
5.2	Methodology . . . . .	17
5.3	Results . . . . .	18
<b>6</b>	<b>IFREMER</b>	<b>24</b>
6.1	Rotor Blade Description . . . . .	24
6.2	Methodology . . . . .	25
6.3	Results . . . . .	25
<b>7</b>	<b>Results</b>	<b>30</b>
<b>8</b>	<b>Conclusions</b>	<b>31</b>
<b>9</b>	<b>Further Work</b>	<b>32</b>
	<b>References</b>	<b>34</b>

## List of Tables

1	Summary of the four BEMT cases. . . . .	4
2	Detailed geometric description of the Magallanes ATIR turbine rotor blade. . . . .	9
3	Details of the flow conditions used in each diagram in the Magallanes ATIR turbine rotor blade analysis. . . . .	11
4	Summary of maximum scaled coefficient of power results for the Magallanes ATIR turbine rotor blade from BEMT cases 1, 2, 3, and 4, and laboratory testing. . . . .	16
5	Detailed geometric description of the Sabella D12 turbine rotor blade. . . . .	17
6	Details of the flow conditions used in each diagram in the Sabella D12 turbine rotor blade analysis. . . . .	18
7	Summary of maximum scaled torque results for the Sabella D12 turbine rotor blade from BEMT case 1, BEMT case 3, and laboratory testing. . . . .	23
8	Detailed geometric description of the IFREMER turbine rotor blade. . . . .	24
9	Details of the flow conditions used in each diagram in the IFREMER turbine rotor blade analysis. . . . .	25
10	Summary of maximum coefficient of power results for the IFREMER turbine rotor blade from BEMT cases 1, 2, 3, and 4, and laboratory testing. . . . .	27

## List of Figures

1	Energy extracting actuator disk and stream-tube. . . . .	2
2	Blade element velocities and forces. . . . .	3
3	Representation of the interpolation table used in assigning unique lift and drag curves to each element in the BEMT model. . . . .	6
4	Schematic of the IFREMER wave and current flume tank used in the laboratory testing of the Magallanes ATIR, Sabella D12, and IFREMER turbine rotor blades. . . . .	7
5	Cross-sectional drawing for each element of the blade profile from the Magallanes ATIR turbine rotor blade. . . . .	10
6	Schematic of the Magallanes ATIR tidal stream device. . . . .	10
7	Scaled Magallanes ATIR turbine model used in laboratory testing. . . . .	10
8	Scaled plot of coefficient of power against tip speed ratio for laboratory results for the Magallanes ATIR turbine rotor at various flow speeds and turbulent intensities. . . . .	12

9 Reynolds number against rotor radial distance for the Magallanes ATIR rotor blade at free flow speeds of  $1.0m.s^{-1}$  and  $1.4m.s^{-1}$  at TSR of 4.75. . . . . 13

10 Scaled plot of coefficient of power against tip speed ratio from BEMT cases 1, 2, 3, and 4 and laboratory results in flow case 1 for the Magallanes ATIR turbine rotor blade. . . . . 13

11 Scaled plot of coefficient of power against tip speed ratio from BEMT cases 1, 2, 3, and 4 and laboratory results in flow case 2 for the Magallanes ATIR turbine rotor blade. . . . . 14

12 Scaled plot of coefficient of power against tip speed ratio from BEMT cases 1, 2, 3, and 4 and laboratory results in flow case 3 for the Magallanes ATIR turbine rotor blade. . . . . 14

13 Scaled plot of coefficient of power against tip speed ratio from BEMT cases 1, 2, 3, and 4 and laboratory results in flow case 4 for the Magallanes ATIR turbine rotor blade. . . . . 15

14 Scaled plot of coefficient of power against tip speed ratio from BEMT cases 1, 2, 3, and 4 and laboratory results in flow case 5 for the Magallanes ATIR turbine rotor blade. . . . . 15

15 Scaled plot of coefficient of power against tip speed ratio from BEMT cases 1, 2, 3, and 4 and laboratory results in flow case 6 for the Magallanes ATIR turbine rotor blade. . . . . 16

16 Proposed design of the Sabella D12 seabed mounted tidal stream turbine. . . . . 17

17 Plot of scaled torque against TSR for laboratory results for the Sabella D12 rotor at various flow speeds and turbulent intensities. . . . . 19

18 Reynolds Number against rotor radial distance for the Sabella D12 rotor blade at free flow speeds of  $0.8m.s^{-1}$ ,  $1.0m.s^{-1}$ , and  $1.4m.s^{-1}$  at TSR of 3.8. . . . . 20

19 Scaled plot of torque against tip speed ratio from BEMT cases 1 and 3 and laboratory results in flow case 1 for the Sabella D12 turbine rotor blade. . . . . 20

20 Scaled plot of torque against tip speed ratio from BEMT cases 1 and 3 and laboratory results in flow case 2 for the Sabella D12 turbine rotor blade. . . . . 21

21 Scaled plot of torque against tip speed ratio from BEMT cases 1 and 3 and laboratory results in flow case 3 for the Sabella D12 turbine rotor blade. . . . . 21

22 Scaled plot of torque against tip speed ratio from BEMT cases 1 and 3 and laboratory results in flow case 4 for the Sabella D12 turbine rotor blade. . . . . 22

23 Scaled plot of torque against tip speed ratio from BEMT cases 1 and 3 and laboratory results in flow case 5 for the Sabella D12 turbine rotor blade. . . . . 22

24	Scaled plot of torque against tip speed ratio from BEMT cases 1 and 3 and laboratory results in flow case 6 for the Sabella D12 turbine rotor blade. . . . .	23
25	Picture of the IFREMER turbine used in laboratory testing.	24
26	Plot of coefficient of power against TSR for laboratory results for the IFREMER turbine at various flow speeds and turbulent intensities. . . . .	26
27	Reynolds Number against rotor radial distance for the IFREMER rotor blade at free flow speeds of $0.6m.s^{-1}$ and $1.0m.s^{-1}$ at TSR of 4.25. . . . .	27
28	Plot of coefficient of power against tip speed ratio from BEMT cases 1, 2, 3, and 4 and laboratory results in flow cases 1 for the IFREMER turbine rotor blade. . . . .	28
29	Plot of coefficient of power against tip speed ratio from BEMT cases 1, 2, 3, and 4 and laboratory results in flow cases 2 for the IFREMER turbine rotor blade. . . . .	28
30	Plot of coefficient of power against tip speed ratio from BEMT cases 1, 2, 3, and 4 and laboratory results in flow cases 3 for the IFREMER turbine rotor blade. . . . .	29
31	Plot of coefficient of power against tip speed ratio from BEMT cases 1, 2, 3, and 4 and laboratory results in flow cases 4 for the IFREMER turbine rotor blade. . . . .	29
32	Plot of scaled coefficient of power against tip speed ratio in flow condition of free stream velocity of $1.0m.s^{-1}$ and turbulence intensity of 15% for BEMT case 1, BEMT case 4, and laboratory results for the Magallanes ATIR and IFREMER turbine rotor blades and BEMT case 1, BEMT case 3, and laboratory results for the Sabella D12 turbine rotor blade. . .	31

## Nomenclature

### Abbreviations

ADV	Acoustic Doppler Velocimeter
BEMT	Blade Element Momentum Theory
CFD	Computational Fluid Dynamics
EMEC	European Marine Energy Centre
IFREMER	French Research Institute for Exploitation of the Sea
LCOE	Levelised Cost of Energy
LDV	Laser Doppler Velocimeter
TEC	Tidal Energy Converter
TI	Turbulence Intensity
TSR	Tip Speed Ratio

TST Tidal Stream Turbine

WP Work Package

### Symbols

$\alpha$	Angle of attack	°
$\Omega$	Tangential speed of rotor blade	$rad.s^{-1}$
$\omega$	Increase in tangential velocity	$rad.s^{-1}$
$\phi$	Inclination of the resultant flow	°
$\theta$	Comined pitch and twist of rotor blade	°
$\nu$	Kinematic viscosity	$m^2.s^{-1}$
$a$	Axial induction factor	—
$b$	Tangential induction factor	—
$c$	Chord length of element	$m$
$Cd$	Drag coefficient	—
$Cl$	Lift coefficient	—
$Cp$	Coefficient of power	—
$dD$	Element drag force	$N$
$dL$	Element lift force	$N$
$L$	Characteristic linear dimension	$m$
$R$	Rotor blade radius	$m$
$r$	Element radial distance along rotor blade	$m$
$T$	Torque	$N.m$
$t$	Thickness of element	$m$
$U$	Free stream velocity	$m.s^{-1}$
$U_{\infty}$	Flow speed far upstream	$m.s^{-1}$
$U_D$	Flow speed at actuator disk	$m.s^{-1}$
$V$	Resultant flow	$m.s^{-1}$

## 1 Introduction

Tidal Stream Turbines (TSTs), also interchangeably called tidal energy converters (TECs), have the potential to become significant contributors of clean renewable energy, reducing our dependency on fossil fuels [1, 2]. Generating energy from the tide has a distinct advantage of being very predictable compared to other renewable energy sources such as wind, solar or wave [2]. Estimations of potential tidal energy in the United Kingdom are between  $50.2 - 95TWh/yr$ ,  $105.4TWh/yr$  in Western Europe, and  $500 - 1000TWh/yr$  worldwide [1, 2]. A significant barrier for TSTs is the expense of operations at sea; more specifically the expense of planned and unplanned maintenance [3–5]. Improving the design of TSTs to minimise the number of planned and unplanned maintenance will greatly increase their popularity.

Blade Element Momentum Theory (BEMT) is a common numerical model that is used for design and performance evaluation of TSTs [6]. BEMT is often the preferred numerical model as it offers acceptable accuracy for evaluation of turbine design iterations with significant computational saving [7–10]. In a computationally efficient manner, BEMT calculates the performance of a turbine or propeller by combining two methods; the momentum "*actuator disk*" theory and the blade element theory [11–13].

A robust BEMT model has been developed at Swansea University [7, 14], which will be the foundation of this work. Previous versions of the BEMT model only allowed for constant geometry and Reynolds Number modelling of the turbine rotor blade, i.e single lift and drag curves for all elements across the radius of the rotor blade. No rotor blade has a constant blade profile and Reynolds Number across its radius which leads to inaccuracies in the results when using the BEMT model. Implementing the capability of assigning unique lift and drag curves to each element based on its geometry and Reynolds Number in the BEMT model will improve the blade geometry modelling, and thus the turbine performance predictions.

Improvements in the accuracy and of the BEMT model will directly enhance the design and evaluation of TSTs. A reduction in levelised cost of energy (LCOE) from TSTs will be seen with a better design which is achievable from the more accurate BEMT model. This will increase the popularity of TSTs as generators of clean renewable energy.

## 2 Blade Element Momentum Theory

BEMT is a common numerical model that is available for predicting the performance of TSTs [6]. It was originally developed in the late 19<sup>th</sup> century for marine and aviation propellers, before being applied to wind turbines and later tidal turbines [11, 13]. BEMT is often the preferred numerical model

for predicting the performance of TSTs as it offers acceptable accuracy for evaluation at low computational cost [7,8,10]. In a computationally efficient manner, the BEMT model calculates the performance of a turbine by combining two methods; the momentum "actuator disk" theory and the blade element theory [13,15]. The following is a brief description of the BEMT model as detailed descriptions are commonly available [13,15].

The momentum theory assumes a stream-tube with a frictionless permeable actuator disk that represents the rotor as shown in Fig.1. It is assumed that the actuator disk does not interact with fluid outside of the stream-tube. Energy is removed from the stream-tube by drag force produced by the actuator disk.

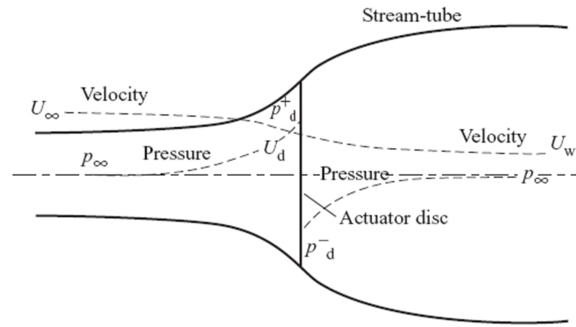


Figure 1: Energy extracting actuator disk and stream-tube.

There are two parts to the momentum theory; linear and rotational theories which differentiate by the assumption of the interaction of the actuator disk and the flow. In linear momentum theory the actuator disk is assumed to induce no rotational velocity to the flow whilst in the rotational momentum theory the actuator disk is assumed to induce rotation to the flow. Bernoulli's equation is used as the foundations in deriving equations for axial force and torque for the rotor blade. Two important factors are introduced; the axial induction factor (1),  $a$ , and the tangential induction factor (2),  $b$ . The axial induction factor,  $a$ , represents the fractional reduction in flow speed from far upstream,  $U_\infty$ , to the flow speed at the actuator disk,  $U_D$ , whilst the tangential induction factor,  $b$ , represents the change in tangential velocity of the flow before and after the actuator disk.

$$a = 1 - \frac{U_D}{U_\infty} \quad (1)$$

$$b = \frac{\omega}{2\Omega} \quad (2)$$

where  $\omega$  is the increase in tangential velocity and  $\Omega$  is the tangential speed of the rotor.

The blade element theory divides the rotor blade into two-dimensional elements along its length. There is no interaction between the elements and thus the loads on the blades can be assumed to rely solely on the lift and drag characteristics of the blade shape. Fig.2 is a diagram showing velocities and forces for a blade element at radius  $r$  relative to the blade chord line.  $\theta$ ,  $\alpha$ , and  $\phi$  represent combined pitch and twist of the blade, angle of attack of the blade from the resultant flow, and inclination of the resultant flow respectively.  $dL$  and  $dD$  are the element lift and drag forces respectively whilst  $V$  is the resultant flow. Axial force and torque for the rotor blade are found by resolving the lift and drag forces.

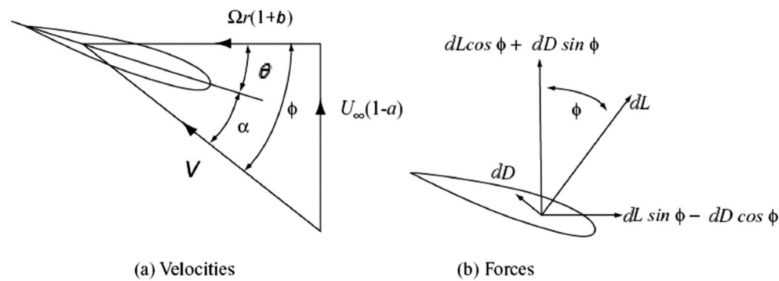


Figure 2: Blade element velocities and forces.

Two formulae for element axial force and torque now exist, derived from two theories. These equations are combined into a single minimisation function and solved [7]. Once the minimisation function is solved, the remaining performance characteristics of the rotor are straightforward to calculate.

### 3 BEMT Procedure

#### 3.1 Cases

Four BEMT cases will be tested, with each successive case increasing the accuracy of the blade geometry modelling. The first BEMT case will use a single lift and drag curves for all elements, the “*original*” model. The second case will allow unique lift and drag curves to be assigned to each element based on their geometry profile. Similarly, the third case will allow unique lift and drag curves to be assigned to each element but will be based on their Reynolds Number alone. The fourth case combines the second and third cases, allowing for unique lift and drag curves to be assigned to each element based on their geometry and Reynolds Number. Summary of the four BEMT cases is shown in Table 1.

Results from the four BEMT cases will be compared to laboratory testing to quantify any improvements in the predicted turbine performance of the

Table 1: Summary of the four BEMT cases.

Case	Geometry dependant?	Reynolds Number dependant?
1	✗	✗
2	✓	✗
3	✗	✓
4	✓	✓

BEMT model. Simulation parameters for the BEMT cases will be dictated by the available laboratory data for each of the analysed turbine rotor blades. Flow conditions, in particular free stream velocity and turbulence intensity have a significant impact on rotor performance. The BEMT cases will use synthetic flow fields which will statistically match the flow fields used in the laboratory testing.

Each BEMT case will be run for 10 seconds at tip speed ratios (TSR) ranging between 2–8. Plots of power coefficient ( $C_p$ ) against TSR will be produced, which will be directly compared to the laboratory results.

### 3.2 Synthetic Flow Fields

The accuracy of the BEMT model in predicting the rotor performance is directly correlated to the precision of the synthetic flow field in representing the physical flow field. Synthetic flow fields used in this work will be produced using the Sandia Method [16–18]. This method produces three-dimensional flow fields that are non-physical, but match statistical properties of real flow at low computational expense [16, 17, 19–22].

There are several options available for the user when creating synthetic flow fields that dictate their statistical properties. Mean longitudinal velocity, turbulence intensity, and size are some basic options available when creating the flow fields. Number of vertical and lateral points are also specified along with the length (*duration*) and timestep of the flow field. Increasing the number of points increases the accuracy of the flow field but also the required computational power. There are options when creating the flow fields to select the streamwise integral lengthscale. Selecting the most appropriate values for these options is important and has significant influence of the quality of the produced synthetic flow field [16–24].

Synthetic flow fields used in this work used 21 points in the vertical and lateral direction, duration of 10s and a timestep of 0.01s. Their streamwise integral lengthscale is set to 0.2 times the turbine rotor diameter which was found to be the most suitable option in a previous study [17]. The remaining options: mean longitudinal velocity, turbulence intensity, and size, matched

the measured laboratory flow field statistical properties.

### 3.3 Implementation

Assigning unique lift and drag curves to each element in the BEMT model is achieved with a relatively simple and minimal code. One of the main strengths of the BEMT model is its low computational demands and thus care is needed when introducing additional features. A brief description of each step in the BEMT model is included below with emphasis placed on the additional geometry modelling feature. The core of the BEMT model used in this work follows the same procedure as any other basic BEMT model and thus detail descriptions of these steps are omitted from this description.

1. Import data
  - Synthetic flow field
  - Rotor blade geometry
2. Loop over blade elements
  - 1 Assume values for two induction factors: axial ( $a$ ) and tangential ( $b$ )
  - 2 Calculate:
    - Relative velocity
    - Angle of attack
    - Reynolds Number
  - 3 ***Assign unique lift and drag curves to each element***
  - 4 Calculate new values for the induction factors  $a$  and  $b$
  - 5 Feed these values back in as the starting values in 2.1 and repeat the process until a converged solution is obtained
3. Induction factors  $a$  and  $b$  are read to the post processor which calculates the load for each blade element and any subsequent parameters

Inclusion of the new geometry modelling feature is achieved in step 2.3. Prior to this step, single lift and drag curves are assigned for all elements for preliminary calculations. Following the calculation of Reynolds Number across the rotor blade, unique lift and drag curves are assigned to each element. Two tables are populated prior to the start of the BEMT model, one with lift curves and one with drag curves. Interpolation of these tables take place during step 2.3, which depends on the Reynolds Number and geometry of each element. Precisely, the lift and drag curves that populate the tables are lift and drag coefficients against angle of attack. Representation of the interpolation tables is shown in Fig.3.

		Blade profile (e.g % thickness/chord)					
		100	45	30	27	24	20
Re ( $1 \times 10^5$ )	6	-	-	-	-	-	-
	5	-	-	-	-	-	-
	4	-	-	-	-	-	-
	3	-	-	-	-	-	-
	2	-	-	-	-	-	-
	1	-	-	-	-	-	-

Figure 3: Representation of the interpolation table used in assigning unique lift and drag curves to each element in the BEMT model.

### 3.4 Calculation of Reynolds Number

Reynolds Number, which is necessary in assigning accurate unique lift and drag curves to each element in step 2.3 is calculated using equation 3. Calculation of fluid velocity with respect to the rotor blade, equation 4, is required prior to the calculation of Reynolds Number. At each time step, Reynolds Number for all elements is calculated, stored, and used in the assigning unique lift and drag curves.

The extent that the Reynolds Number changes between time steps across the turbine rotor blade is correlated to the turbulence intensity of the flow field. Higher turbulence flow fields result in greater Reynolds Number change which will increase the scatter in the predicted performance results from the BEMT model.

$$Re = \frac{VL}{\nu} \quad (3)$$

$$V = \sqrt{U^2 + (\Omega R)^2} \quad (4)$$

- $V$  = Instantaneous fluid velocity with respect to the rotor blade ( $m.s^{-1}$ )
- $L$  = Characteristic linear dimension [i.e. half rotor blade chord length] ( $m$ )
- $\nu$  = Kinematic viscosity ( $m^2.s^{-1}$ )
- $U$  = Free stream velocity ( $m.s^{-1}$ )
- $\Omega$  = Rotational speed of the rotor blade ( $rad.s^{-1}$ )
- $R$  = Rotor blade length ( $m$ )

### 3.5 Creation of Lift and Drag Data

Curves of lift and drag coefficients against angle of attack is specifically what is required for the BEMT model. The coefficients against angle of attack will populate the interpolation table. They will be produced predominantly by computational fluid dynamics (CFD) simulations, but with some being extrapolated from experimental testing. The CFD simulations uses the forceCoeffs function which generates aerodynamic force and moment coefficients data for surfaces and porous regions, and is available from OpenFoam [25].

### 3.6 Laboratory Testing

Experimental testing of the Magallanes ATIR, Sabella D12, and IFREMER turbine rotors were carried out by University Le Havre Normandy, France at IFREMER wave and flume tank in Boulogne-Sur-Mer, France. Detailed description of the IFREMER wave and current flume tank laboratory facility can be found in previous works [20, 26–29]. A schematic of the IFREMER wave and current flume tank is shown in Fig.4 [26].

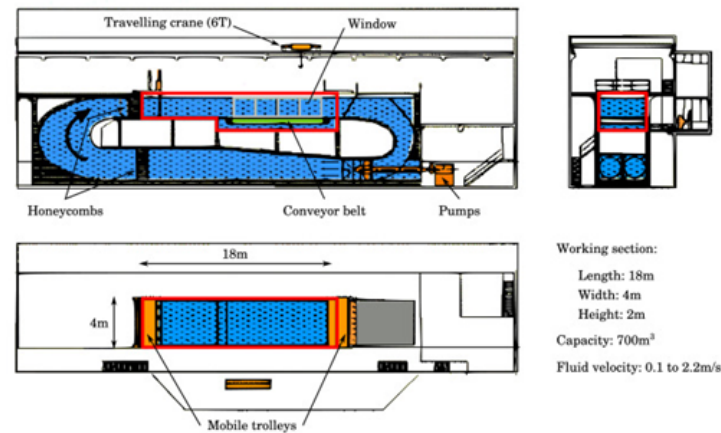


*Figure 4:* Schematic of the IFREMER wave and current flume tank used in the laboratory testing of the Magallanes ATIR, Sabella D12, and IFREMER turbine rotor blades.

During laboratory testing it is imperative that data for the flow condition and rotor performance is accurately collected. Imprecise laboratory data would present misleading conclusions when comparing to BEMT predictions. Flow velocity and turbulence intensity are the important flow condition parameters that are needed to be known for the BEMT model. These parameters are measured using laser doppler velocimeter (LDV) and acoustic doppler velocimeter (ADV). Torque and thrust measurements for the rotor are directly measured on the rotation axis which eliminates nacelle or support drag in recorded data. Each blade is fitted with a five-component

load-cell at their root which measures two forces and three moments. The rotor is mounted to a motor-gearbox assembly which allows accurate control of its rotational speed.

A limitation of the laboratory facility is the available flow conditions that are attainable. Flow speeds are generally limited to the range of  $0.8m.s^{-1}$  –  $1.4m.s^{-1}$  which equates to a Reynolds Number range of  $2.7 \times 10^5$  –  $4.7 \times 10^5$ . Turbulence intensities of 1.3%, 1.5%, 3%, 5%, and 15% are attainable in the wave and current flume tank with a combination of flow straightening meshes.

## 4 Magallanes ATIR

### 4.1 Rotor Blade Description

The Magallanes ATIR tidal stream device is a floating structure which has two three-bladed turbines. The profile of the rotor blades are based on the NACA 63418 aerofoil but varies across their radius, from a cylinder at their hub to a thin section at their tip. Each rotor blade is represented by twelve elements in the BEMT model. Detail descriptions for all elements are given in Table 2, specifically their radius ( $r$ ) and chord ( $c$ ) with respect to rotor radius ( $R$ ), pitch in degrees, and thickness ( $t$ ) to chord as a percentage. Element 1 represents the inner-most section the rotor blade, its root, whilst element 12 represents the outer-most section of the rotor blade, its tip. Cross-sectional blade profile drawings for each element is shown in Fig.5. Figures 6 and 7 show a schematic of the Magallanes ATIR tidal stream device and a scaled turbine model used in the laboratory testing respectively.

Table 2: Detailed geometric description of the Magallanes ATIR turbine rotor blade.

Element	$r/R$	$c/R$	Pitch ( $deg$ )	$t/c$ (%)
1	0.1263	0.1368	-	100
2	0.1579	0.1368	-	100
3	0.1789	0.1368	-	100
4	0.2316	0.2444	17.9	43.1
5	0.3368	0.2048	12.5	35.4
6	0.4421	0.1845	10.5	30.7
7	0.5474	0.1583	8.6	28.0
8	0.6526	0.1270	7.1	27.8
9	0.7579	0.0982	6.0	26.8
10	0.8632	0.0759	5.2	24.3
11	0.9158	0.0659	4.7	22.2
12	1.000	0.0532	4.3	17.4

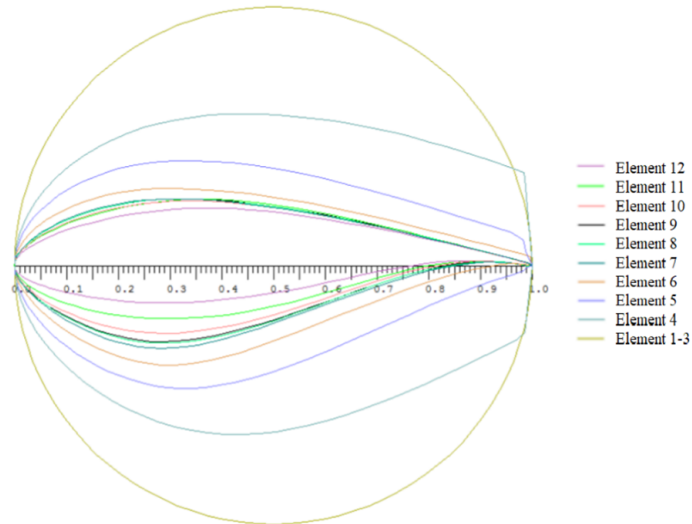


Figure 5: Cross-sectional drawing for each element of the blade profile from the Magallanes ATIR turbine rotor blade.



Figure 6: Schematic of the Magallanes ATIR tidal stream device.



Figure 7: Scaled Magallanes ATIR turbine model used in laboratory testing.

## 4.2 Methodology

All four BEMT cases will be tested, made possible by the varying profile of the Magallanes ATIR turbine rotor blades. Improvements to the geometry modelling of the ATIR turbine rotor blades in the BEMT model will be concerned with both varying blade geometry and Reynolds Number. Rotor performance results from the BEMT model will be compared to laboratory testing to quantify the effects of geometry profile and Reynolds Number variance in the BEMT model.

Six different flow conditions will be used for analysis which have different combination of flow speeds and turbulent intensities. A diagram with results from all four BEMT cases and laboratory testing will be produced for each flow conditions. Specifically, the diagrams will plot rotor blade  $C_p$  against TSR. Optimum rotational rate of the Magallanes ATIR turbine rotor will be

deduced from laboratory testing and will be used as the point of comparison between cases. Details of the flow conditions for each diagram is tabulated in Table 3. The flow conditions used in the analysis are limited to those achievable in the laboratory testing, due to the necessity of the laboratory results to quantify any improvements to the BEMT model.

Table 3: Details of the flow conditions used in each diagram in the Magallanes ATIR turbine rotor blade analysis.

Flow cases	Flow speed	Turbulent intensity	<u>Legend</u>	
1	Low	Low	<u>Flow speed</u>	<u>Turbulence intensity</u>
2	Low	Medium	–Low = $1.0m.s^{-1}$	–Low = 1.3%
3	Low	High	–High = $1.4m.s^{-1}$	–Medium = 5.0%
4	High	Low		–High = 15.0%
5	High	Medium		
6	High	High		

### 4.3 Results

All results have been scaled to ensure commercial sensitivity is maintained. This is achieved by dividing all  $C_p$  values by the maximum  $C_p$  value in the plot.

Plot of scaled coefficient of power against tip speed ratio results from laboratory testing for the Magallanes ATIR turbine rotor at various flow speeds and turbulent intensities is shown in Fig.8. Six curves are plotted which represent each of the flow cases stated previously. Rotor performance increases significantly with flow speed whilst little change is seen with different turbulent intensities. Optimum rotor performance is seen at TSR of 5.0 for flow speed of  $1.0m.s^{-1}$  and at TSR of 4.5 for flow speed of  $1.4m.s^{-1}$ .

Reynolds Number across the Magallanes ATIR turbine rotor blade has been calculated for flow speeds of  $1.0m.s^{-1}$  and  $1.4m.s^{-1}$  at TSR of 4.75. A plot of Reynolds Number against rotor blade radial distance is shown in Fig.9. There is very little difference in Reynolds Number variance across rotor blade radius at different turbulence intensities and thus not included in the diagram.

As expected, the Reynolds Number distribution across the rotor blade is the same at different flow speeds and differs only in magnitude. The Reynolds Number distribution for the Magallanes ATIR turbine rotor blade increases from its minimum at the blade root to its maximum around the mid rotor radius length, element 7, and then decreases towards the rotor tip. Minimum Reynolds Number is approximately 40% of the maximum value, seen at the

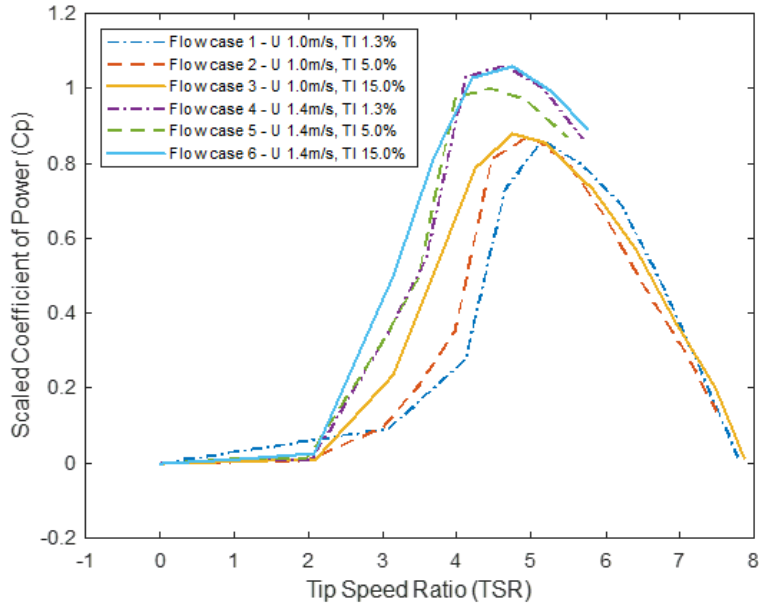


Figure 8: Scaled plot of coefficient of power against tip speed ratio for laboratory results for the Magallanes ATIR turbine rotor at various flow speeds and turbulent intensities.

rotor hub, and the Reynolds Number at the rotor tip is approximately 60% of the maximum value.

Scaled  $C_p$  against TSR for each tested flow cases for BEMT cases 1 – 4 and laboratory results are shown in Figs.(10-15) respectively. Summary and comparison of the maximum scaled  $C_p$  results can be found in Table 4. As previously stated, each diagram represents different flow cases which differ by free stream velocity and turbulence intensity. Results for all diagrams follow the same trend and have similar curves with the only major difference being the magnitude, which is predominantly influenced by free stream flow speed.

All BEMT cases over-predict the performance of the turbine. BEMT case 1 is the most inaccurate in matching the laboratory results followed closely by case 3, with the difference exaggerated in over rotation operation ( $TSR > 4.75$ ). Considerable improvement in matching laboratory results over the whole tested TSR range is seen by BEMT cases 2 and 4, with case 4 always being the best match.

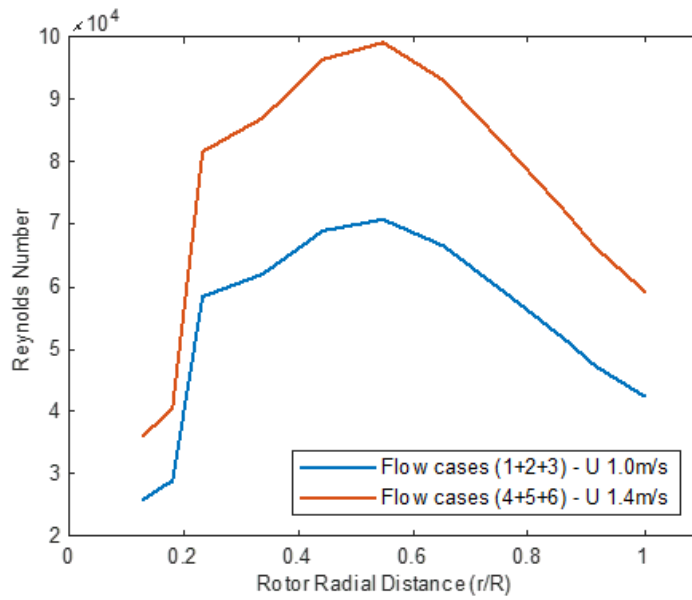


Figure 9: Reynolds number against rotor radial distance for the Magallanes ATIR rotor blade at free flow speeds of  $1.0m.s^{-1}$  and  $1.4m.s^{-1}$  at TSR of 4.75.

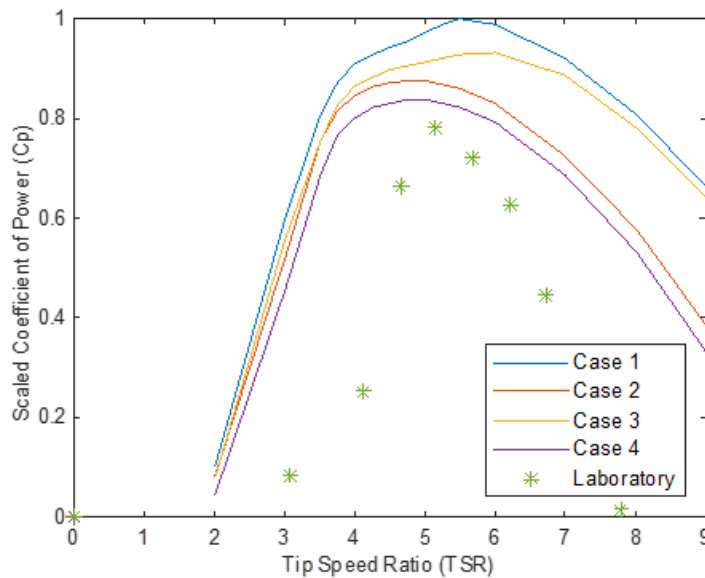


Figure 10: Scaled plot of coefficient of power against tip speed ratio from BEMT cases 1, 2, 3, and 4 and laboratory results in flow case 1 for the Magallanes ATIR turbine rotor blade.

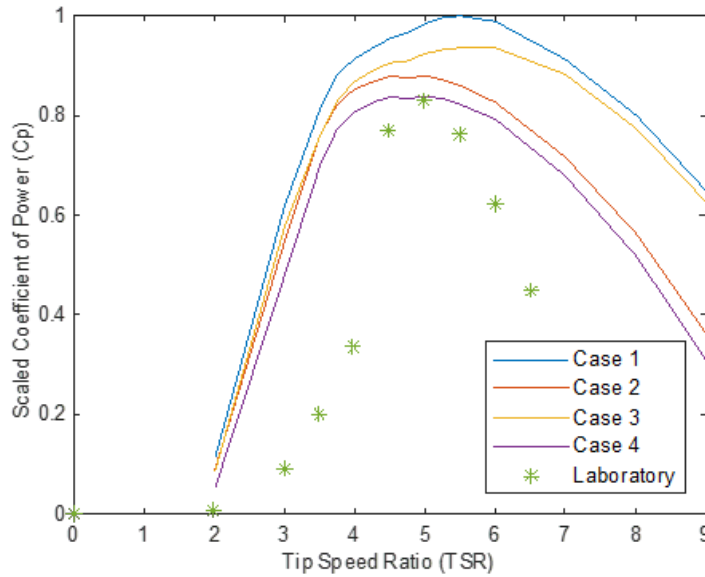


Figure 11: Scaled plot of coefficient of power against tip speed ratio from BEMT cases 1, 2, 3, and 4 and laboratory results in flow case 2 for the Magallanes ATIR turbine rotor blade.

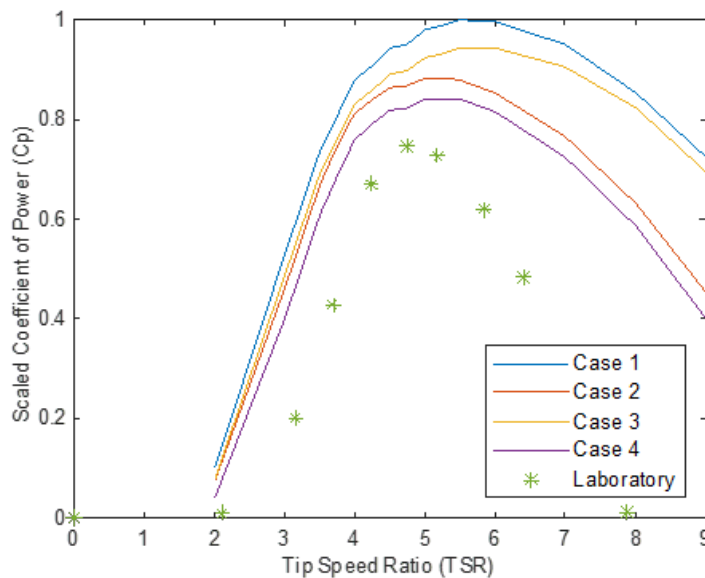


Figure 12: Scaled plot of coefficient of power against tip speed ratio from BEMT cases 1, 2, 3, and 4 and laboratory results in flow case 3 for the Magallanes ATIR turbine rotor blade.

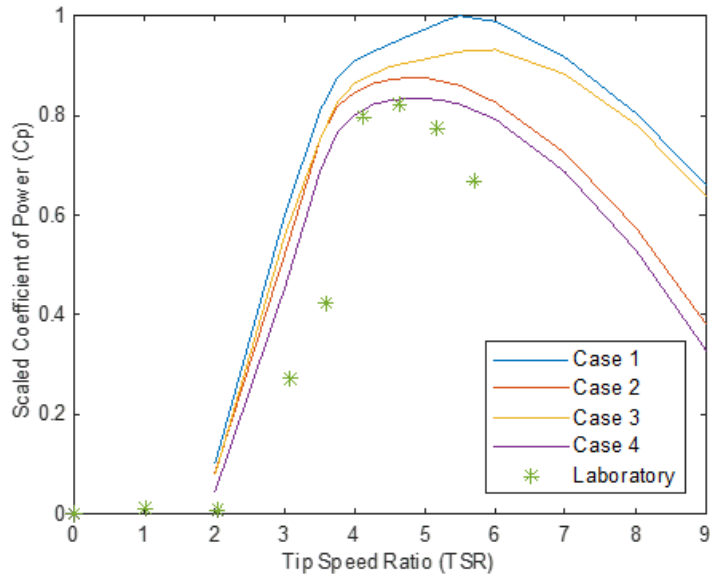


Figure 13: Scaled plot of coefficient of power against tip speed ratio from BEMT cases 1, 2, 3, and 4 and laboratory results in flow case 4 for the Magallanes ATIR turbine rotor blade.

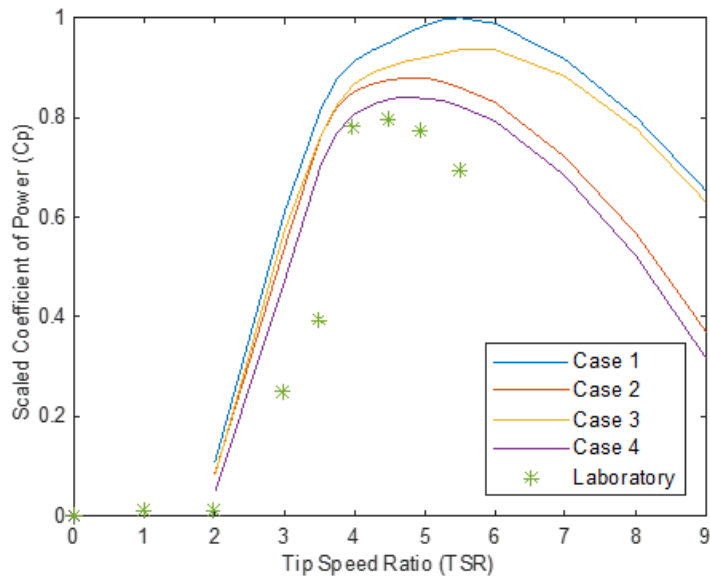


Figure 14: Scaled plot of coefficient of power against tip speed ratio from BEMT cases 1, 2, 3, and 4 and laboratory results in flow case 5 for the Magallanes ATIR turbine rotor blade.

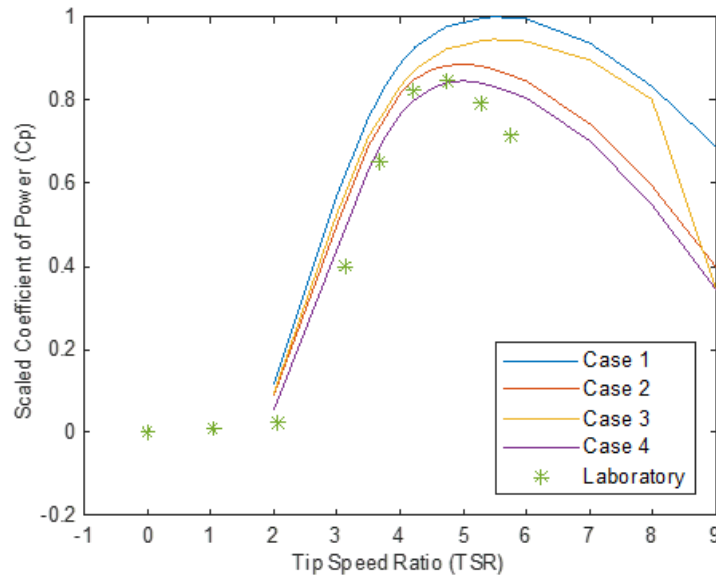


Figure 15: Scaled plot of coefficient of power against tip speed ratio from BEMT cases 1, 2, 3, and 4 and laboratory results in flow case 6 for the Magallanes ATIR turbine rotor blade.

Table 4: Summary of maximum scaled coefficient of power results for the Magallanes ATIR turbine rotor blade from BEMT cases 1, 2, 3, and 4, and laboratory testing.

Flow cases	Maximum scaled coefficient of power					Difference in maximum coefficient of power to laboratory (%)			
	BEMT case				Laboratory	BEMT case			
	1	2	3	4		1	2	3	4
1	1.000	0.873	0.934	0.834	0.780	+28.2	+12.0	+19.7	+6.9
2	1.000	0.880	0.937	0.842	0.832	+20.2	+5.7	+12.5	+1.1
3	1.000	0.887	0.946	0.844	0.748	+33.7	+18.6	+26.5	+12.9
4	1.000	0.874	0.933	0.835	0.822	+21.6	+6.3	+13.5	+1.6
5	1.000	0.881	0.936	0.841	0.796	+25.7	+10.7	+17.7	+5.7
6	1.000	0.886	0.944	0.843	0.846	+18.2	+4.7	+11.6	-0.3

## 5 Sabella D12

### 5.1 Rotor Blade Geometry

The Sabella D12 tidal stream turbine has 5 rotor blades which have a constant 15% elliptical profile across their radius. Each rotor blade is represented by 32 elements in the BEMT model. Detail descriptions for seven of the elements are given in Table 5, specifically their radius ( $r$ ) with respect to rotor radius ( $R$ ) and chord ( $c$ ) with respect to rotor maximum chord ( $C$ ). Element 1 represents the inner-most section the rotor blade, its root, whilst element 32 represents the outer-most section of the rotor blade, its tip. Figure 16 depicts the proposed design of the Sabella D12 seabed mounted tidal stream turbine [30].

*Table 5:* Detailed geometric description of the Sabella D12 turbine rotor blade.

Element	$r/R$	$c/C$
1	0.321	1.000
6	0.423	0.673
11	0.536	0.519
16	0.649	0.424
21	0.762	0.360
26	0.875	0.320
32	1.000	0.300

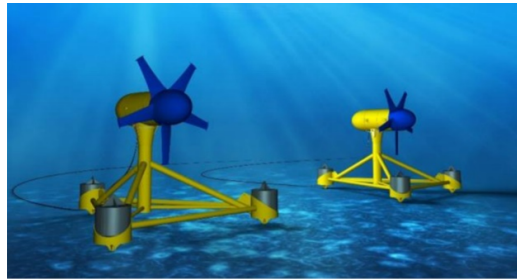


*Figure 16:* Proposed design of the Sabella D12 seabed mounted tidal stream turbine.

### 5.2 Methodology

Due to the constant elliptical profile of the D12 rotor blade, there is no scope to introduce varying blade geometry into the BEMT model. Improvements to the blade geometry modelling of the D12 rotor blade in the BEMT model will solely be concerned with varying Reynolds Number. Rotor performance results from the BEMT model will be compared to laboratory testing to quantify the effects of introducing Reynolds Number variance.

Six different flow conditions will be used for analysis which covers a range of flow speeds and turbulent intensities. A diagram with results from the BEMT case 1, BEMT case 3, and laboratory testing will be produced for each of the flow conditions. Specifically, the diagrams will plot torque ( $T$ ) against TSR. Optimum rotation rate of the D12 turbine will be deduced from laboratory testing and will be used as the point of comparison between cases. Detail of the flow conditions for each diagram is tabulated in Table 6.

Table 6: Details of the flow conditions used in each diagram in the Sabella D12 turbine rotor blade analysis.

Flow cases	Flow speed	Turbulent intensity	<u>Legend</u>	
1	<i>Low</i>	<i>Low</i>	<u>Flow speed</u>	<u>Turbulence intensity</u>
2	<i>Low</i>	<i>High</i>	– <i>Low</i> = $0.8m.s^{-1}$	– <i>Low</i> = 1.5%
3	<i>Medium</i>	<i>Low</i>	– <i>Medium</i> = $1.0m.s^{-1}$	– <i>High</i> = 15.0%
4	<i>Medium</i>	<i>High</i>	– <i>High</i> = $1.4m.s^{-1}$	
5	<i>High</i>	<i>Low</i>		
6	<i>High</i>	<i>High</i>		

### 5.3 Results

All results have been scaled to ensure commercial sensitivity is maintained. This is achieved by dividing all torque values by the maximum torque value in the plot.

Plot of scaled torque against TSR for laboratory results of the Sabella D12 turbine rotor at various flow speeds and turbulent intensities is shown in Fig.17. Six curves are plotted which are for each of the flow conditions stated previously. Both flow speed and turbulent intensity influence the rotor performance. Higher flow speed results in increased rotor performance whilst an increase in turbulent intensity decreases the rotor performance. Optimum rotor performance is seen at TSR of 3.8 for all flow conditions. Torque is used for the analysis of the Sabella D12 turbine rotor blade rather than power, as used for the Magallanes ATIR turbine, due to the available laboratory data.

Figure 18 shows the Reynolds Number against rotor blade radial distance for the Sabella D12 tidal stream turbine at three flow speeds of  $0.8m.s^{-1}$ ,  $1.0m.s^{-1}$ , and  $1.4m.s^{-1}$  at TSR of 3.8. Plots with the same flow velocities are combined as turbulence intensity has little effect on the Reynolds Number.

As expected, the Reynolds Number distribution across the rotor blade is the same at different flow speeds and differs only in magnitude. Maximum Reynolds Number is seen at the blade root, in element 1. It decreases to its minimum value, which is 70% of the maximum, at 80% of the rotor blade radius in element 23, and then increases to 75% of the maximum value at the rotor blade tip.

The Reynolds Number across the Sabella D12 turbine rotor blade varies by 30%, which is a comparable small range and is likely to result in minimum improvements in the BEMT model rotor performance predictions.

Scaled torque against TSR for each tested flow conditions for BEMT cases

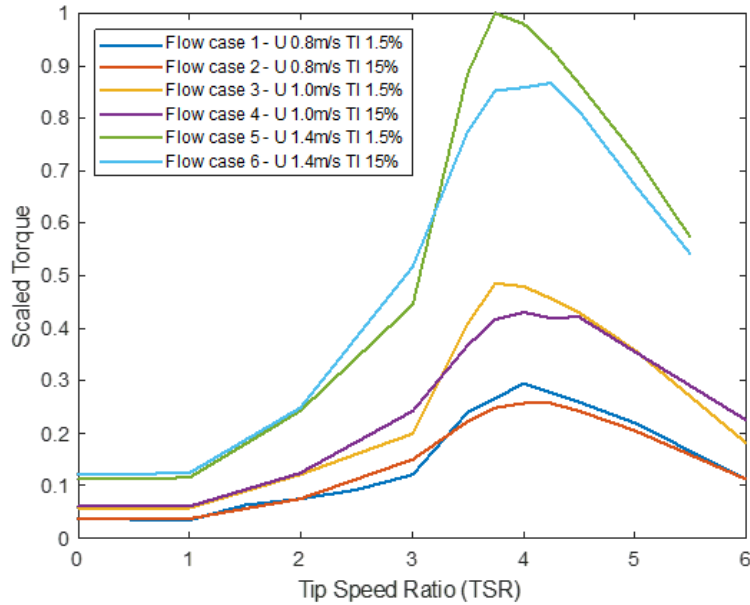


Figure 17: Plot of scaled torque against TSR for laboratory results for the Sabella D12 rotor at various flow speeds and turbulent intensities.

1 and 3 and laboratory results are shown in Figs.(19-24) respectively. Summary of the maximum scaled torque results can be found in Table 7. As previously stated, each diagram represents different flow conditions which differ by free stream flow velocity and turbulence intensity.

Results for all diagrams follow the same trend and have similar curves with the only major difference being the magnitude, which is predominantly influenced by free stream flow speed. The BEMT case 1 and BEMT case 3 have similar results due to the relatively small Reynolds Number variance across the rotor blade. Prior to optimum rotor operating speed, BEMT case 1 predicts slightly higher torque values than BEMT case 3, whilst after optimum rotor operating speed BEMT case 3 predicts higher torque than BEMT case 1. At optimum rotor operating speed, both BEMT cases predict higher torque values than recorded in the laboratory testing. In every tested flow condition BEMT case 1 predicts higher maximum torque values than BEMT case 3.

Turbulence intensity of the flow field has a significant impact on the difference in maximum torque predicted by the BEMT cases and what is recorded from laboratory testing. In low and medium flow speeds, the difference in maximum torque values of the BEMT and laboratory results are significantly larger in the higher turbulence intensity flow conditions. In the high flow speed cases, the difference in maximum torque values of the BEMT cases and the laboratory results decrease slightly with higher turbulent intensity.

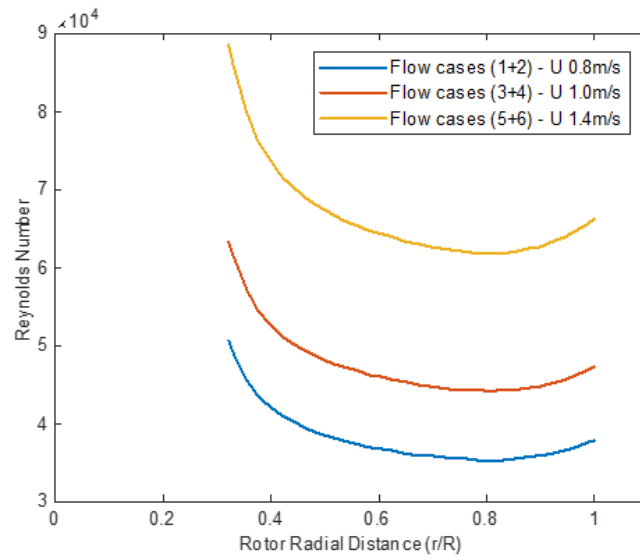


Figure 18: Reynolds Number against rotor radial distance for the Sabella D12 rotor blade at free flow speeds of  $0.8\text{m}\cdot\text{s}^{-1}$ ,  $1.0\text{m}\cdot\text{s}^{-1}$ , and  $1.4\text{m}\cdot\text{s}^{-1}$  at TSR of 3.8.

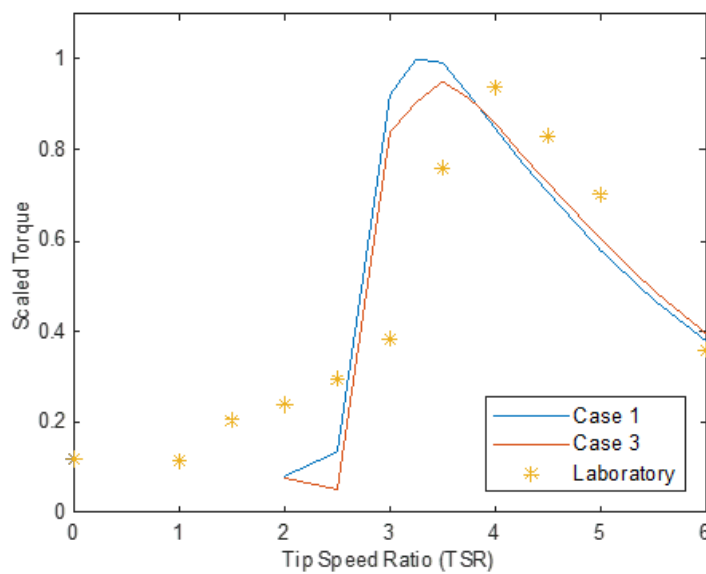


Figure 19: Scaled plot of torque against tip speed ratio from BEMT cases 1 and 3 and laboratory results in flow case 1 for the Sabella D12 turbine rotor blade.

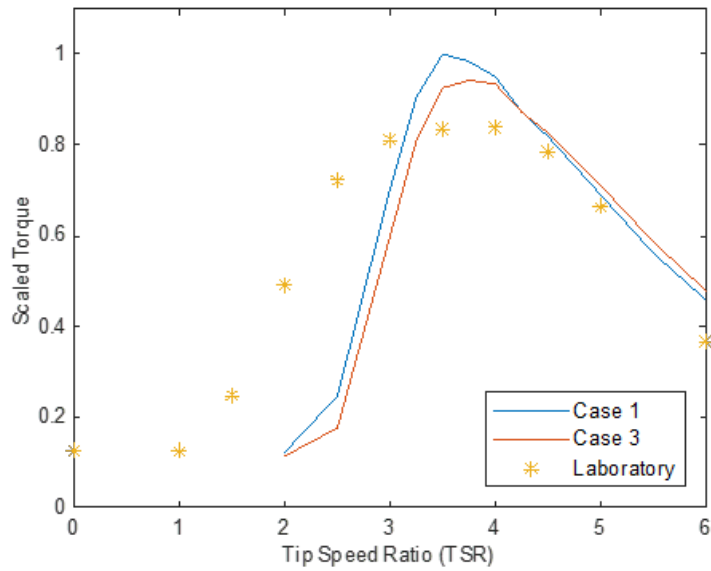


Figure 20: Scaled plot of torque against tip speed ratio from BEMT cases 1 and 3 and laboratory results in flow case 2 for the Sabella D12 turbine rotor blade.

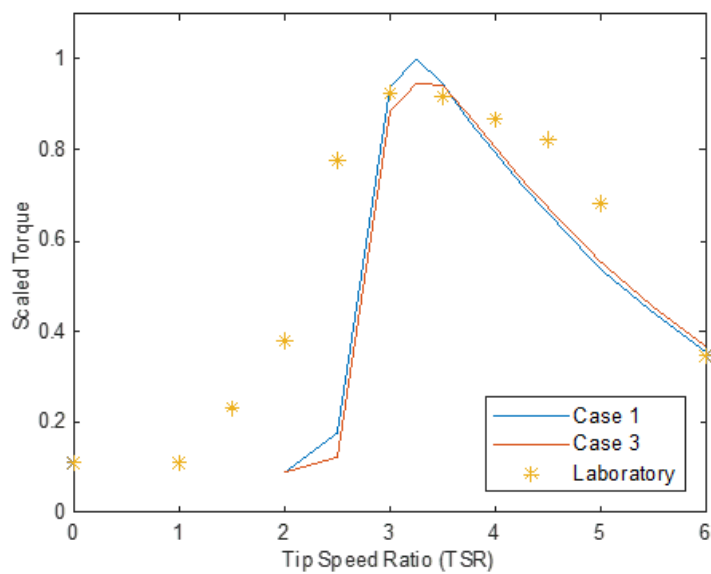


Figure 21: Scaled plot of torque against tip speed ratio from BEMT cases 1 and 3 and laboratory results in flow case 3 for the Sabella D12 turbine rotor blade.

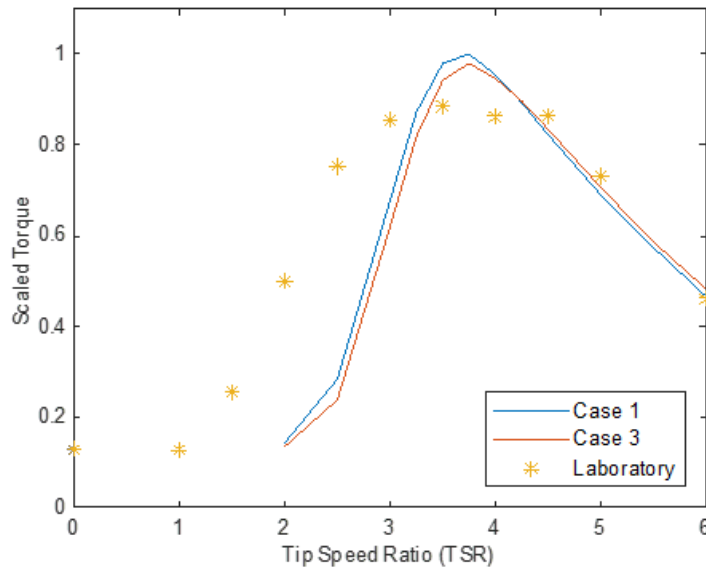


Figure 22: Scaled plot of torque against tip speed ratio from BEMT cases 1 and 3 and laboratory results in flow case 4 for the Sabella D12 turbine rotor blade.

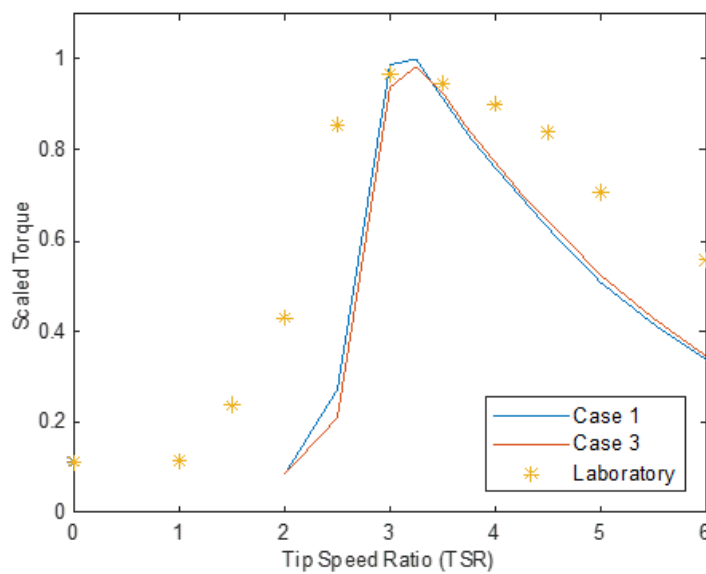


Figure 23: Scaled plot of torque against tip speed ratio from BEMT cases 1 and 3 and laboratory results in flow case 5 for the Sabella D12 turbine rotor blade.

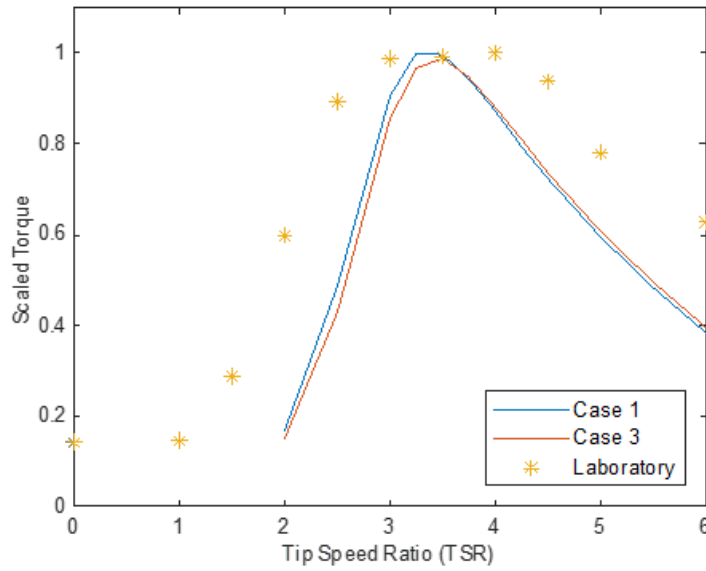


Figure 24: Scaled plot of torque against tip speed ratio from BEMT cases 1 and 3 and laboratory results in flow case 6 for the Sabella D12 turbine rotor blade.

Table 7: Summary of maximum scaled torque results for the Sabella D12 turbine rotor blade from BEMT case 1, BEMT case 3, and laboratory testing.

Flow cases	Maximum scaled torque			Difference in maximum torque to laboratory (%)	
	BEMT case		Laboratory	BEMT case	
	1	3		1	3
1	1.000	0.951	0.938	+6.6	+1.4
2	1.000	0.942	0.839	+19.2	+12.4
3	1.000	0.947	0.925	+5.6	+2.4
4	1.000	0.978	0.884	+13.1	+10.6
5	1.000	0.984	0.967	+3.4	+1.8
6	0.996	0.981	1.000	-0.6	-1.9

## 6 IFREMER

### 6.1 Rotor Blade Description

The IFREMER tidal stream turbine has 3 rotor blades which are designed based on the NACA 63418 aerofoil profile. The profile of the rotor blades varies across their radius, which starts as a cylinder at the root and thins towards the tip. Each rotor blade is represented by 23 elements in the BEMT model. Detail descriptions for ten of the elements are given in Table 8, specifically their radius ( $r$ ) and chord ( $c$ ) with respect to rotor radius ( $R$ ), pitch in degrees, and thickness ( $t$ ) to chord as a percentage. Element 1 represents the inner-most section the rotor blade, at its root, whilst element 23 represents the outer-most section of the rotor blade, at its tip. The turbine used in the laboratory and BEMT testing in the following work has a rotor radius of  $362\text{mm}$  and a hub radius of  $55\text{mm}$ . Figure 25 shows the IFREMER turbine used for laboratory testing [29].

Table 8: Detailed geometric description of the IFREMER turbine rotor blade.

Element	$r/R$	$c/R$	Pitch ( $deg$ )	$t/c$ (%)
1	0.1333	0.0567	29.5672	80.0
2	0.1500	0.0567	29.5672	100.0
3	0.1550	0.0567	29.5672	100.0
4	0.1983	0.1521	25.6273	36.0
5	0.2417	0.2472	22.1491	21.3
10	0.4583	0.1925	12.1169	22.4
15	0.6750	0.1529	7.8191	21.9
20	0.8917	0.1285	5.6050	18.6
22	0.9783	0.1213	5.0143	18.0
23	1.000	0.0655	4.8743	25.0



Figure 25: Picture of the IFREMER turbine used in laboratory testing.

## 6.2 Methodology

All four BEMT cases will be tested, made possible by the varying profile of the IFREMER turbine rotor blade. Improvements to the geometry modelling of the IFREMER turbine rotor blade in the BEMT model will be concerned with both varying blade geometry and Reynolds Number. Rotor performance results from the BEMT model will be compared to laboratory testing to quantify the effects of geometry profile and Reynolds Number variance in the BEMT model.

Four different flow conditions will be used for analysis which have different combination of flow speeds and turbulent intensities. A diagram with results from all four BEMT cases and laboratory testing will be produced for each of the flow conditions. Specifically, the diagrams will plot rotor  $C_p$  against TSR. Optimum rotation rate of the IFREMER turbine will be deduced from laboratory testing and will be used as the point of comparison between cases. Detail of the flow conditions for each diagram is tabulated in Table 9. The flow conditions used in the analysis are limited to those used in the laboratory testing, due to the need for laboratory testing results for quantifying improvements to the BEMT model.

Table 9: Details of the flow conditions used in each diagram in the IFREMER turbine rotor blade analysis.

Flow cases	Flow speed	Turbulent intensity	<i>Legend</i>	
1	<i>Low</i>	<i>Low</i>	<u>Flow speed</u>	<u>Turbulence intensity</u>
2	<i>Low</i>	<i>High</i>	– <i>Low</i> = $0.6m.s^{-1}$	– <i>Low</i> = 3.0%
3	<i>High</i>	<i>Low</i>	– <i>High</i> = $1.0m.s^{-1}$	– <i>High</i> = 15.0%
4	<i>High</i>	<i>High</i>		

## 6.3 Results

Plots of  $C_p$  against TSR for laboratory results of the IFREMER turbine at various flow speeds and turbulent intensities are shown in Fig.26. Four curves are plotted which represent each of the flow conditions stated previously. As with other turbines, both flow speed and turbulent intensity influence the rotor performance. Increase in flow speed increases the rotor performance whilst an increase in turbulent intensity decreases the rotor performance. Optimum rotor performance is seen approximately at TSR of 4.0 and 4.5 for flow conditions with speeds of  $0.6m.s^{-1}$  and  $1.0m.s^{-1}$  respectively. Comparison of BEMT and laboratory cases will be made at TSR of 4.25.

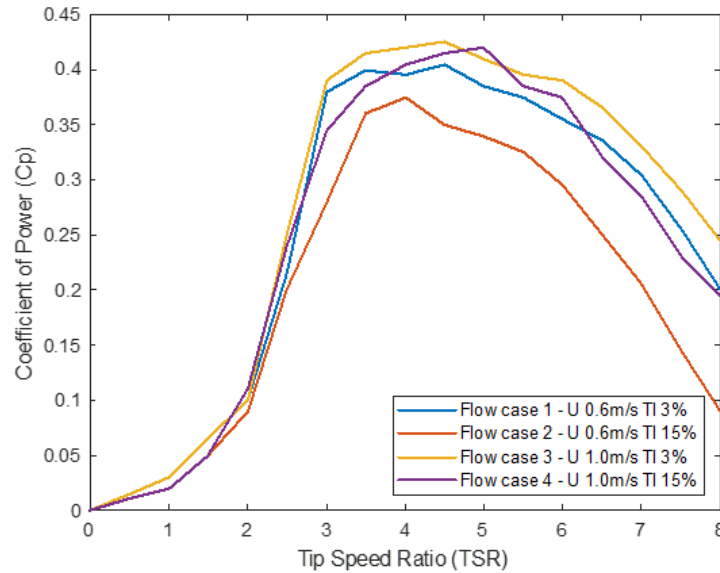


Figure 26: Plot of coefficient of power against TSR for laboratory results for the IFREMER turbine at various flow speeds and turbulent intensities.

Reynolds Number across the IFREMER turbine rotor blade has been calculated for flow speeds of  $0.6m.s^{-1}$  and  $1.0m.s^{-1}$  at TSR of 4.25. A plot of Reynolds Number against rotor blade radial distance is shown in Fig.27. There is very little difference in Reynolds Number variance across rotor blade radius at different turbulence intensities and thus not included in the diagram.

As expected, the Reynolds Number distribution across the rotor blade is the same at different flow speeds and differs only in magnitude as is seen in the other rotor blades. The Reynolds Number distribution for the IFREMER turbine rotor blade increases from its minimum at the hub to its maximum just prior to the tip. A significant drop in Reynolds Number is seen at the tip element due to a rapid change in rotor blade geometry. Minimum Reynolds Number is 13% of the maximum value, which gives a large range that will provide significant scope for BEMT improvements.

$C_p$  against TSR for each tested flow conditions for BEMT cases 1 – 4 and laboratory results are shown in Figs.(28-31) respectively. Summary and comparison of the maximum  $C_p$  results can be found in Table 10. As previously stated, each diagram represents different flow conditions which differ by free stream velocity and turbulence intensity.

Results for the BEMT cases follow the same trend across the different flow conditions. Prediction of rotor performance is always highest in BEMT case 1, followed by case 3, case 2, and finally case 4. There is very little difference between rotor performance prediction results from BEMT cases 2

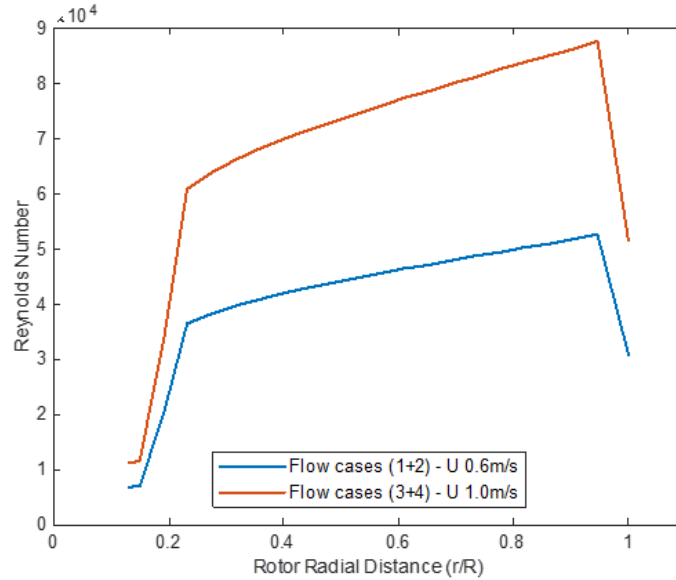


Figure 27: Reynolds Number against rotor radial distance for the IFREMER rotor blade at free flow speeds of  $0.6m.s^{-1}$  and  $1.0m.s^{-1}$  at TSR of 4.25.

and 4. Generally, the BEMT cases underpredict the rotor performance when compared to laboratory results. The best correlation between the BEMT cases and laboratory results is seen at the higher turbulence intensity flow conditions.

Table 10: Summary of maximum coefficient of power results for the IFREMER turbine rotor blade from BEMT cases 1, 2, 3, and 4, and laboratory testing.

Flow cases	Maximum coefficient of power					Difference in maximum coefficient of power to laboratory (%)			
	BEMT case				Laboratory	BEMT case			
	1	2	3	4		1	2	3	4
1	0.396	0.355	0.382	0.351	0.405	-2.2	-12.3	-5.7	-13.3
2	0.435	0.389	0.414	0.383	0.375	+16.0	+3.7	+10.4	+2.1
3	0.408	0.366	0.393	0.361	0.425	-4.0	-13.9	-7.5	-15.1
4	0.439	0.392	0.416	0.386	0.420	+4.6	-6.7	-1.0	-8.1

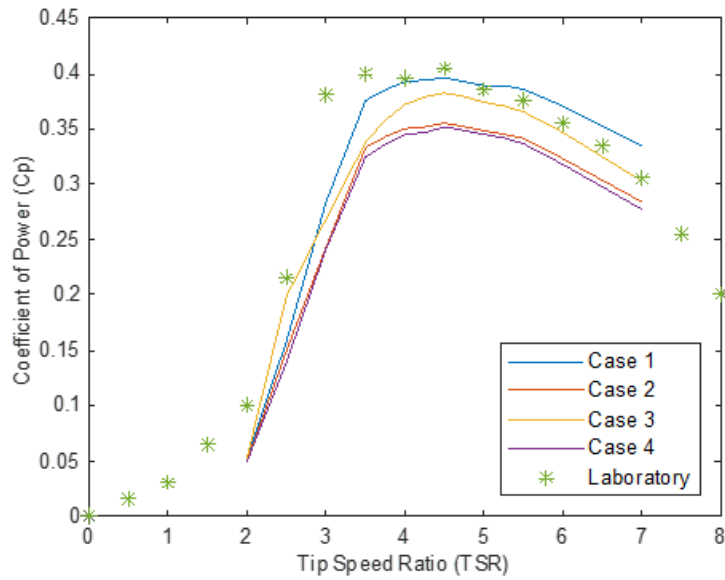


Figure 28: Plot of coefficient of power against tip speed ratio from BEMT cases 1, 2, 3, and 4 and laboratory results in flow cases 1 for the IFREMER turbine rotor blade.

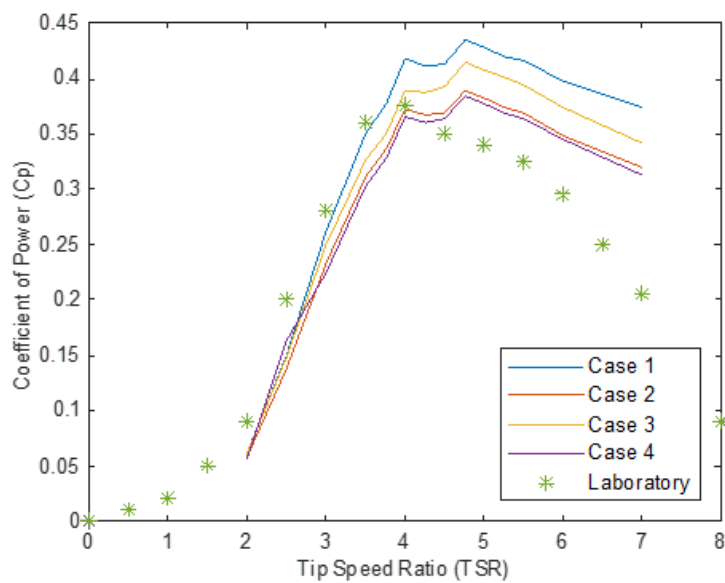


Figure 29: Plot of coefficient of power against tip speed ratio from BEMT cases 1, 2, 3, and 4 and laboratory results in flow cases 2 for the IFREMER turbine rotor blade.

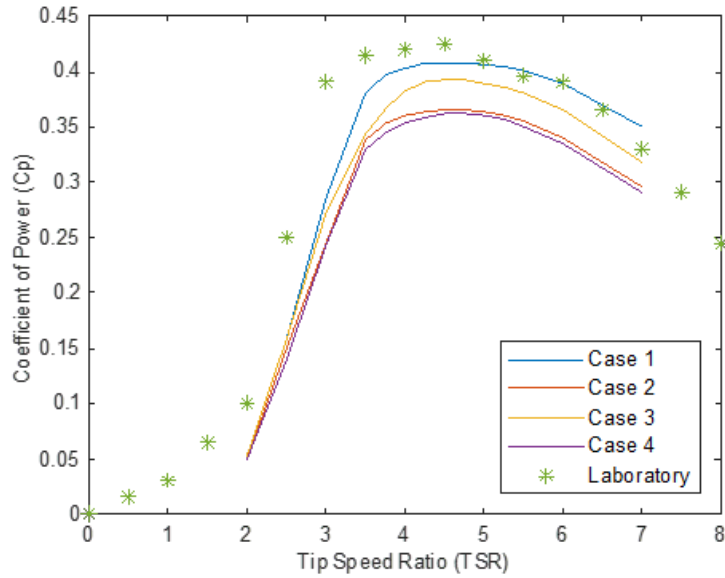


Figure 30: Plot of coefficient of power against tip speed ratio from BEMT cases 1, 2, 3, and 4 and laboratory results in flow cases 3 for the IFREMER turbine rotor blade.

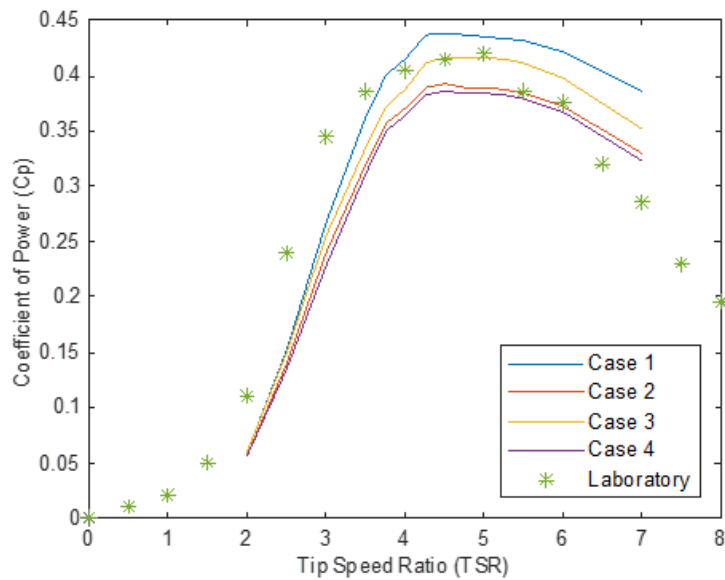


Figure 31: Plot of coefficient of power against tip speed ratio from BEMT cases 1, 2, 3, and 4 and laboratory results in flow cases 4 for the IFREMER turbine rotor blade.

## 7 Results

Full analysis has been undertaken on the Magallanes ATIR and IFREMER turbine rotor blades, made possible due to their varying blade geometry. In the BEMT model, the rotor blades are modelled using single lift and drag curves for all elements in case 1 whilst in case 4 each element is assigned unique lift and drag curves based on their geometry and Reynolds Number. Using unique lift and drag curves for each element is a more accurate representation on the rotor blades and should improve the performance prediction of the BEMT model. Due to the constant geometry profile of the Sabella D12 turbine rotor blades, it was only possible to use BEMT cases 1 and 3 in its analysis, the inclusion of Reynolds Number dependency.

As is seen in all results, BEMT case 4 always predicts lower turbine rotor performance compared to BEMT case 1. This can be explained by the geometry of the rotor blades which has been previously described in detail. In BEMT case 1 all elements are assumed to have the same lift and drag characteristic which is inaccurate. Both the ATIR and IFREMER rotor blades have circular profile at their roots which gradually thins to their main profile. Accurately portraying the lift and drag characteristics of all elements across the rotor blades, as is achieved in BEMT case 4, decreases the predicted performance of the turbine rotor which is mainly due to the lower performance of the inner most elements which were previously being represented as having performance closer to the outboard elements with better hydrodynamic characteristics.

Although we expect that the accuracy of rotor blade modelling in the BEMT model is better in BEMT case 4 compared to the original BEMT case 1, improvement in comparison to laboratory results is not always seen. The best match to the laboratory results is always seen with the most accurate BEMT geometry modelling model for the Magallanes ATIR and Sabella D12 turbine rotors. The IFREMER turbine rotor results are not as straightforward, with the best match to laboratory results seen with different BEMT cases depending on the flow conditions. The closest match to the laboratory results is seen with BEMT case 4 for the high turbulence (15%) flow conditions and BEMT case 1 for the low turbulence (3%) flow conditions.

A plot of scaled  $C_p$  against TSR for all rotor blades is shown in Fig.32. The analysis was completed in flow conditions of  $1.0m.s^{-1}$  free stream velocity and 15% turbulence intensity. BEMT case 1, BEMT case 4, and laboratory results are included for the Magallanes ATIR and IFREMER turbine rotors and BEMT case 1, BEMT case 3, and laboratory results for the Sabella D12 turbine rotor. As is expected, BEMT case 4 predicts lower rotor performance compared to BEMT case 1 for the ATIR and IFREMER turbines. There is very little difference between BEMT cases for the D12 turbine due to the constant geometry of its rotor blade and minimal Reynolds Number change. An improvement of 20% in predicting laboratory maximum rotor

performance results is seen for the ATIR turbine rotor from BEMT case 1 to BEMT case 4. Accuracy in matching the laboratory maximum rotor performance result for the IFREMER rotor decreases by 3% from the BEMT case 1 and BEMT case 4. Although the accuracy in predicting maximum rotor performance decreases between BEMT case 1 and 4 for the IFREMER rotor, the rotor prediction between tip speed ratio of 3 to 7 has improved by 5%.

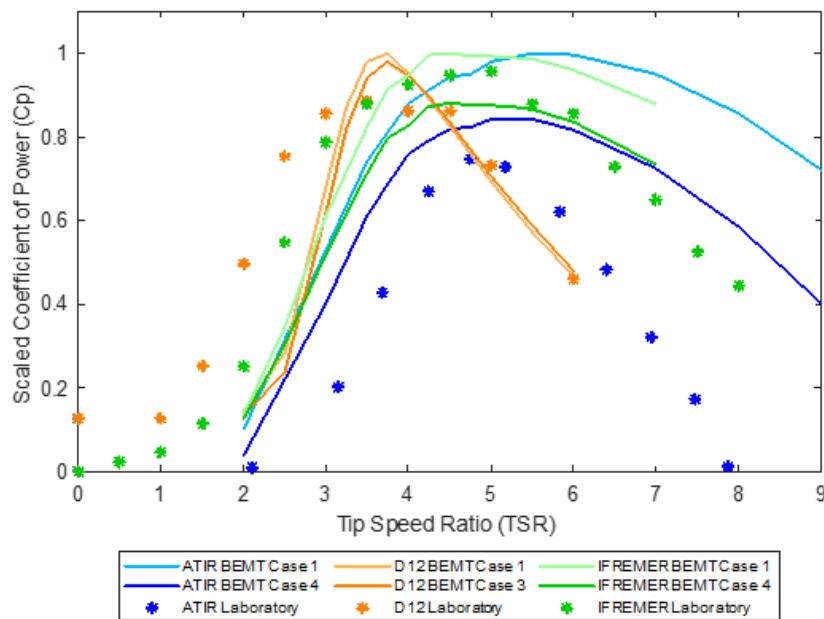


Figure 32: Plot of scaled coefficient of power against tip speed ratio in flow condition of free stream velocity of  $1.0m.s^{-1}$  and turbulence intensity of 15% for BEMT case 1, BEMT case 4, and laboratory results for the Magallanes ATIR and IFREMER turbine rotor blades and BEMT case 1, BEMT case 3, and laboratory results for the Sabella D12 turbine rotor blade.

## 8 Conclusions

Rotor blade geometry modelling in the BEMT model has been improved by introducing the ability to assign unique lift and drag curves to each element. Comparison of BEMT rotor performance prediction with and without the improved blade geometry modelling has been made against laboratory results. In the majority of cases, the BEMT model with the advanced blade geometry modelling reproduce closer results to those of the laboratory testing.

BEMT model prediction of maximum rotor performance to laboratory results has improved by an average of 20.0% and 4.6% respectively for the Magallanes ATIR and Sabella D12 turbine rotor blades whilst it has decreased by 3.0% for the IFREMER turbine rotor with the inclusion of the improved blade geometry modelling.

Comparing BEMT cases 2 and 3, it is clear to see that including geometry dependence has significantly greater impact on the BEMT model than that of Reynolds Number dependence. Including geometry dependence compared to Reynolds Number dependence has an average of 40% greater improvement in BEMT rotor performance prediction to laboratory. This is unsurprising as there is a more significant change in geometry than Reynolds Number across the rotor blades.

In every tested case the BEMT models which include the improved blade geometry modelling predict reduced rotor performance. This is due to accurate assignment of lift and drag curves to each BEMT element. BEMT elements in the original model, particular ones towards the blade hub, were assigned lift curves which were inappropriate and overpredicted their performance.

The flow conditions and synthetic flow fields both have significant impact on the BEMT results. Rotor performance is positively correlated to free stream velocity whilst turbulence intensity has a relative negligible effect. Using accurate synthetic flow fields in the BEMT model is crucial in ensuring useful prediction of rotor performance. It is imperative that the synthetic flow fields match statistical properties of the real flows.

Introducing the improved blade geometry modelling to the BEMT model has increased the computational time by approximately 10%. This is an acceptable increase in computational time in respect to added accuracy of the blade geometry modelling and the BEMT model prediction of rotor performance.

Increasing the accuracy of the BEMT model in predicting tidal stream turbine rotor performance will result in improved rotor blade design and reliability. This will in turn reduce the cost associated with tidal stream turbines, increasing their adoption as generators of low carbon energy.

## 9 Further Work

As has been made clear throughout this work, the accuracy of the BEMT model is dependent on the synthetic flow field. Sensitivity of the BEMT predicted rotor performance to the synthetic flow field should be undertaken to check the reliability of the results. Such parameters as duration of flow field, size of flow field with respect to turbine rotor, time step size, number of data points, and integral length scale could all be analysed.

Increasing the number of elements used in the BEMT model would increase

the computational time but also the accuracy of the results. Analysis should be carried out to find the optimum number of elements to maximise the accuracy of results to computational demand.

Results and quantification of any improvements of predicting rotor performance from the BEMT model have been made against laboratory testing. At sea testing of both Magallanes ATIR and Sabella D12 tidal stream turbines are currently being performed. Once the trial data become available, comparison will be made to the results predicted by the BEMT model.

## References

- [1] M. Melikoglu, “Current status and future of ocean energy sources: A global review,” *Ocean Engineering*, vol. 148, pp. 563–573, jan 2018.
- [2] R. Pelc and R. M. Fujita, “Renewable energy from the ocean,” *Marine Policy*, vol. 26, pp. 471–479, nov 2002.
- [3] C. Johnstone, D. Pratt, J. Clarke, and A. Grant, “A techno-economic analysis of tidal energy technology,” *Renew Energy*, vol. 49, pp. 101–106, 2013.
- [4] S. Astariz, A. Vazques, and G. Iglesias, “Evaluation and comparison of the levelized cost of tidal, wave and offshore wind energy,” *Journal of Renewable Sustainable Energy*, vol. 7, no. 5, 2015.
- [5] A. Sagar and B. Van Der Zwaan, “Technological innovation in the energy sector: R&D, deployment and learning-by-doing,” *Energy Polivy*, vol. 34, no. 17, pp. 2601–2608, 2006.
- [6] S. Ordonez-Sanchez, R. Ellis, K. E. Porter, M. Allmark, T. O’Doherty, A. Mason-Jones, and C. Johnstone, “Numerical models to predict the performance of tidal stream turbines working under off-design conditions,” *Ocean Engineering*, vol. 181, pp. 198–211, jun 2019.
- [7] I. Masters, J. C. Chapman, M. R. Willis, and J. A. Orme, “A robust blade element momentum theory model for tidal stream turbines including tip and hub loss corrections,” *Journal of Marine Engineering and Technology*, vol. 10, no. 1, pp. 25–35, 2011.
- [8] B. Mannion, S. B. Leen, and S. Nash, “Development and assessment of a blade element momentum theory model for high solidity vertical axis tidal turbines,” *Ocean Engineering*, vol. 197, p. 106918, feb 2020.
- [9] B. Mannion, V. McCormack, S. B. Leen, and S. Nash, “A CFD investigation of a variable-pitch vertical axis hydrokinetic turbine with incorporated flow acceleration,” *Journal of Ocean Engineering and Marine Energy*, vol. 5, no. 1, pp. 21–39, 2019.
- [10] W. M. J. Batten, A. S. Bahaj, A. F. Molland, and J. R. Chaplin, “Experimentally validated numerical method for the hydrodynamic design of horizontal axis tidal turbines,” *Ocean Engineering*, vol. 34, pp. 1013–1020, may 2007.
- [11] E. Houghton and A. Brock, *Aerodynamics for engineering students*. Arnold, 1960.
- [12] P. Moriarty and A. Hansen, *AeroDyn theory manual*. NREL, 2005.

- [13] T. Burton, D. Sharpe, N. Jenkins, and E. Bossanyi, *Wind energy handbook*. 2001.
- [14] J. Chapman, I. Masters, M. Togneri, and J. Orme, “The Buhl correction factor applied to high induction conditions for tidal stream turbines,” *Renewable Energy*, vol. 60, pp. 472–480, dec 2013.
- [15] M. Hansen, *Aerodynamics of wind turbines*. London: Earthscan, 2 ed., 2008.
- [16] M. Togneri, G. Pinon, C. Carlier, C. Choma Bex, and I. Masters, “Comparison of synthetic turbulence approaches for blade element momentum theory prediction of tidal turbine performance and loads,” *Renewable Energy*, vol. 145, pp. 408–418, 2020.
- [17] P. Veers, “Three-dimensional Wind Simulation - Sandia method,” *Journal of Geophysical Research*, vol. 92, no. A3, p. 2289, 1987.
- [18] I. Milne, R. Sharma, R. Flay, and S. Bickerton, “Characteristics of the turbulence in the flow at a tidal stream power site,” *Phil. Trans. Roy. Soc, Lond. A Math. Phys. Eng. Sci.*, vol. 371, 2013.
- [19] T. Stallard, R. Collings, T. Feng, and J. Whelan, “Interactions between tidal turbine wakes: experimental study of a group of three-bladed rotors,” *Philos Trans R Soc*, 2013.
- [20] T. Blackmore, L. Myers, and A. Bahaj, “Effects of turbulence on tidal turbines: Implications to performance, blade loads, and condition monitoring,” *International Journal of Marine Energy*, vol. 14, pp. 1–26, 2016.
- [21] P. Pyakurel, J. VanZwieten, M. Dhanak, and N. Xiros, “Numerical modeling of turbulence and its effect on ocean current turbines,” *International Journal of Marine Energy*, vol. 17, pp. 84–97, 2017.
- [22] N. Jarrin, S. Benhamadouche, D. Laurence, and R. Prosser, “A synthetic-eddy-method for generating inflow conditions for large-eddy simulations,” *International Journal of Heat and Fluid Flow*, vol. 27, no. 4, pp. 585–593, 2006.
- [23] I. Milne, A. Day, R. Sharma, and R. Flay, “The characterisation of the hydrodynamic loads on tidal turbines due to turbulence,” *Renew Sustain Energy*, no. 56, pp. 851–864, 2016.
- [24] T. Blackmore, W. Batten, and A. Bahaj, “Influence of turbulence on the wake of a marine current turbine simulator,” *The royal society*, vol. 470, 2014.

- [25] OpenFoam, “OpenFOAM: Force coefficients.”
- [26] B. Gaurier, C. Carlier, G. Germain, G. Pinon, and E. Rivoalen, “Three tidal turbines in interaction: An experimental study of turbulence intensity effects on wakes and turbine performance,” *Renewable Energy*, vol. 148, pp. 1150–1164, apr 2020.
- [27] F. Maganga, G. Germain, J. King, G. Pinon, and E. Rivoalen, “Experimental characterisation of flow effects on marine current turbine behaviour and on its wake properties,” *IET Renewable Power Generation*, vol. 4, no. 6, pp. 314–327, 2010.
- [28] O. Medina, F. Schmitt, R. Calif, G. Germain, and B. Gaurier, “Turbulence analysis and multiscale correlations between synchronized flow velocity and marine turbine power production,” *Renewable Energy*, vol. 112, pp. 314–327, 2017.
- [29] P. Mycek, B. Gaurier, G. Germain, G. Pinon, and E. Rivoalen, “Experimental study of the turbulence intensity effects on marine current turbines behaviour. Part 1: One single turbine,” *Journal of Renewable Energy*, vol. 66, pp. 729–746, 2014.
- [30] M. Togneri, E. Buck, A. Macleod, E. Nicolas, J. Nuño, and M. O. Connor, “Multi-model analysis of tidal turbine reliability,” 2019.